

Electrochemical sensor for the sensitive detection of *o*-nitrophenol using graphene oxide-poly(ethyleneimine) dendrimer-modified glassy carbon electrode

Tanvir Arfin¹  · Rani Bushra² · Faruq Mohammad³

Received: 22 February 2016/Revised: 19 May 2016/Accepted: 13 July 2016/Published online: 21 July 2016
© Springer International Publishing Switzerland 2016

Abstract The graphene oxide-poly(ethyleneimine) dendrimer (GO-PEI) was synthesized and characterized by SEM, TEM, UV-Vis, FTIR, and Raman spectroscopies and further employed for the fabrication of modified glassy carbon electrode by a drop-cast method. The electrochemical behaviour of ortho-nitrophenol (*o*-NP) was investigated at the modified electrode, and the results of the investigation revealed that the material exhibited a significant reduction capability towards *o*-NP, an indication of sensitive electrochemical response. In addition, the modified electrode possessed an excellent electrochemical behaviour towards the redox of *o*-NP by combining the properties of both GO and PEI. Also, it was found that the *o*-NP can be separated indigenously from different potentials of nitrosophenol or hydroxyl aminophenol redox reaction. The peak currents showed a linear relationship with the concentration of *o*-NP in the range of 5–155 μM . The limit of detection of *o*-NP is low as 0.10 μM characterized by the signal-to-noise characteristics ($S/N = 3$). The relative standard deviation (RSD) for the three times determination towards *o*-NP is 0.12 %, which is highly specified, and reveals that this method has good properties such as reproducibility capability, selectivity, repeatability,

and stability. Hence, the present GO-PEI-based *o*-NP sensors proved to be endeavouring for a broad range of applications related to the detection of trace amounts of phenolic compounds. In addition, the material was successfully employed for the treatment of industrially contaminated water during the removal of heavy metals (Fe^{3+} , Ni^{2+} , Cu^{2+} , Pb^{2+} , and Zn^{2+} ions).

Keywords Graphene oxide · Poly(ethyleneimine) dendrimer · Electrochemical reduction · *O*-nitrophenol · Electrochemical detection

1 Introduction

Phenol and its derivatives are being used for many industrial applications, and because of this reason, its compounds are commonly released into soil, water, and environment in trace amounts. In general, the phenolic compounds are toxic to humans, animals, and plants [1]. One of the phenolic derivatives, *o*-NP, a yellow crystalline solid and steam volatile, is highly toxic and has much more severe impacts on the growth and metabolic activity of the organisms even contaminating the soil near the former explosive [2]. Nitrophenols have been listed as one of the toxic organic pollutants among the top 114 pollutants by the US Environmental Protection Agency because of certain undergoing reason. Therefore, the reduction of *o*-NP is of great interest since it is regarded for pollution decline.

In that view, the current methods of NPs detection include flow injection analysis [3], spectrophotometry [4], high-performance liquid chromatography (HPLC) [5], capillary electrophoresis [6], electrochemical sensors [7], and micro-extraction [8]. The electrochemical behaviour of NPs is very compatible with a series of schemes having

✉ Tanvir Arfin
tanvirarfin@gmail.com

¹ Environmental Materials Division, CSIR-National Environmental Engineering Research Institute (CSIR-NEERI), Nagpur 440020, India

² Analytical Research Laboratory, Department of Chemistry, Aligarh Muslim University, Aligarh 202002, India

³ Surfactants Research Chair, Department of Chemistry, College of Science, King Saud University, P. O. Box 2455, Riyadh 11451, Saudi Arabia

successive reactions which involve proton and electron exchange to produce the corresponding reduced derivatives.

Graphene is a non-metal with a two-dimensional (2D) structure containing three electrons in the sp^2 orbital present in the form in-plane C–C bonds showing the honey comb-like structure where the fourth electron is found to scatter all throughout from the top to the bottom as a π electron resembling C–C bond length of 0.142 nm [9]. The GO obtained from graphene contains oxygen functional groups in the form of epoxy located in the basal plane, hydroxyl, carbonyl, and carboxyl groups situated on the edges of sheets [10]. GO in its pure form as nanocomposite shows a number of applications in various different fields that include electronics, biosensors, fuel cell, catalysis, semiconductors, and packing due to its exceptional electrochemical performance, electron transfer rate, and adsorption/desorption of molecules, in addition to executing some extraordinary physical properties [11–13]. GO and its composites have been applied extensively in a wide range for the adsorption of heavy metal ions (namely Au^{3+} , Pt^{4+} , Cu^{2+} , Cd^{2+} , Zn^{2+} , and Hg^{2+}), enhanced antibacterial activity, and superior electrical conductivities [14].

Dendrimers are regular, a branched tree from core to termini, roughly spherical, vast, 3D macromolecules with well-defined chemical structures, and it gathers attention in biological fields due to its large number of functional groups at the edge [15]. For example, polyethyleneimine (PEI) is among one of the dendritic polymer families consisting of primary amino end groups, secondary amino groups present in the main chain, and tertiary amine in the form of the branch as shown in Fig. 1. PEI molecules show a globular-type structure with slight conformational freedom due to its high degree of branching. PEI is a hyperbranched polymer, available in both forms such as

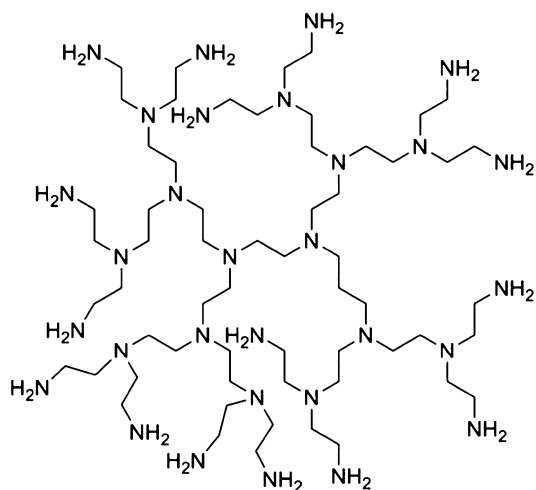


Fig. 1 Chemical structure of PEI

linear and branched showing molecular weights ranging from 200 to 800,000 Da and cationic in nature. The backbone of PEI is made up of vinyl bonds in the form of carbon–carbon linkages resulting in the formation of the non-degradable polymer. Also, due to its active amine groups, PEI can readily react with other materials having carboxyl or epoxy groups, and thus, PEI can be an ideal candidate for the modification of graphene structure.

Electrochemical methods are considered as one of the faster, durable, and cheapest techniques for the quantitative detection and quantitative determination of different species [16]. The determination of *o*-NP was done with the help of several modified electrodes according to the literature studies. But yet there is no report on the application of proposed electrode. Hence, here in this context, an efficient attempt has been made to develop a dendrimer containing a GO-based electrochemical system for the measurement of *o*-NP. For that, we prepared GO–PEI composite, and its properties were studied along with the determination of *o*-NP using a new electrochemical sensor which is based on the drop-cast method of the dendrimer. The reaction mechanism of GO–PEI showed a covalent grafting process of PEI to the graphene sheets as there is a nucleophilic ring-opening reaction of epoxy groups in GO with the amino groups in PEI. For the composite, the smaller size of PEI allows for its deposit within the inter-layer space of GO, thereby sustaining the parallel arrangement of GO sheets even after the composite formation, in addition to allowing for the synthesis reaction without the aid of any coupling agent. Hence, the GO–PEI composite was prepared by the functionalization of GO with that of PEI, and the particular material was utilized to modify the surface of glassy carbon electrode (GCE). The enhancing effect of GO–PEI electrode has an effect on the redox chemistry of ferricyanide and ferrocyanide system which particularly attracted us to apply this electrode system for a substrate like *o*-NP and its quantitative analysis. The composite found to exhibit an excellent electrochemical activity and well-defined reduction peaks with increased peak currents towards *o*-NP. The method seems to be simple, cost-effective, and sensitive as the experimental results show that PEI significantly affects the separation of reduction peak potentials of *o*-NP.

2 Experimental details

2.1 Materials and methods

PEI dendrimer ($M_n = 10,000$ g/mol) (PEI) was purchased from SyMO-Chem (Eindhoven, Netherlands). KH_2PO_4 , K_2HPO_4 , KCl, $K_3[Fe(CN)_6]$, $K_4[Fe(CN)_6]$, and *o*-NP were obtained from Merck (Johannesburg, South Africa).

Natural graphite (flake type, an average size of 45 μm) was purchased from Sigma-Aldrich Inc (Johannesburg, South Africa). The phosphate buffer saline (PBS 10 mM, pH 7.4) with 0.1 M KCl was used as supporting electrolyte. A 5 mM of $\text{K}_3[\text{Fe}(\text{CN})_6]$ and $\text{K}_4[\text{Fe}(\text{CN})_6]$ was prepared in 100 mL of the buffer solution, and ratio of $\text{K}_3[\text{Fe}(\text{CN})_6]$ and $\text{K}_4[\text{Fe}(\text{CN})_6]$ was 1:1. Mill-Q water with a resistance greater than 18 $\text{M}\Omega$ was used all throughout our experiments. All the chemicals are of analytical grade and were used without any further purification.

2.2 Synthesis of GO

The synthesis of GO from natural graphite was adopted from the Hummer's method, but with a slight modification and described elsewhere [17]. In brief, the powdered flake graphite (4 g) was mixed with 160 mL of H_2SO_4 and NaNO_3 (5 g) in an ice bath for 4 h. Now, KMnO_4 (24 g) was slowly added to the mixture and the temperature being maintained at $<20^\circ\text{C}$ so as to avoid the overheating and explosion that can occur during the experimental procedures. The temperature of the solution was increased to 35°C and maintained the same for 2 h, and around 320 mL of distilled water was added to the mixture. Following a 2-h period, the solution was further diluted by pouring an additional 800 mL of water, followed by the slow addition of 24 mL of H_2O_2 (30 %, v/v) which was injected into the solution to enhance the complete reaction with the excess of KMnO_4 . After these steps, the black graphite suspension seems to be converted to a bright yellow graphite oxide solution, and the resulting mixture was washed thoroughly with HCl and water. The precipitate of GO formed was isolated by centrifugation at 3000 rpm/min for around 15 min, washed out, and then re-suspended in water. The obtained GO was dispersed in water having a certain concentration and subsequently sonicated for 2 h to facilitate the exfoliated of stacked GO sheets into monolayer or multi-layered GO sheets having the structural similarities as shown in Fig. 2.

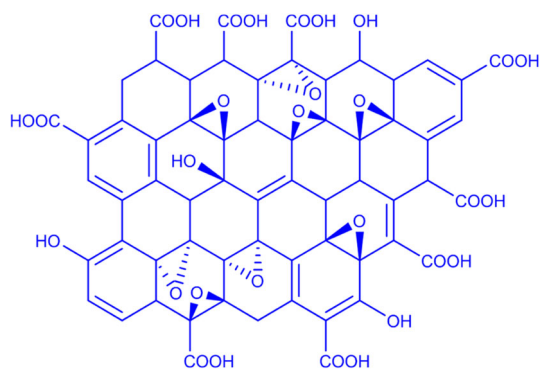


Fig. 2 Chemical structure of GO

Permanganate is a commonly used oxidant (e.g. dihydroxylations), which is an active species and is, in fact, dimanganese heptoxide (Mn_2O_7) (Scheme 1). This dark red oil is formed from the reaction of KMnO_4 with H_2SO_4 gently with each other. The bimetallic heptoxide is said to be far more reactive than its monometallic tetraoxide counterpart and is known to detonate when heated to temperatures greater than 35°C or when placed in contact with organic compounds [18]. Trömel and Russ have demonstrated the ability of Mn_2O_7 to selectively oxidize unsaturated aliphatic double bonds over the aromatic double bonds, which may have important implications and susceptibility towards graphene structure and the reaction pathways occurring during the oxidation [19].

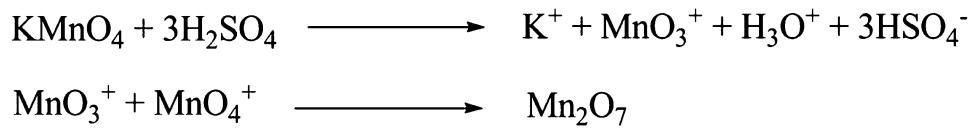
2.3 Synthesis of GO-PEI-modified electrode

The bare GCE was gently polished with 1.0-, 0.3-, and 0.05- μm alpha alumina powder before it was used for the experiment, rinsed ultrasonically with 1:1 HNO_3 , ethanol, and de-ionized water, respectively, and dried at room temperature. GO (1 mL) was dispersed in 1 mL of PEI solution with ultra-sonication for better results. The tentative structure proposed is shown in Scheme 2. Amino-terminated PEI dendrimer was linked through a covalent bond to the surface of GO forming a new amide bond directly grafting PEI at the framework of GO.

About 5 μL of GO-PEI suspension was cast on the surface of bare GCE and dried in air stream for few hours. Prior to use, the modified electrode was carefully rinsed with water to remove the GO-PEI at the electrode which is loosely attached and dried in an air stream. Each electrochemical testing experiment was allocated by a freshly prepared and coated bare glassy electrode which has been working to obtain the reproducible results.

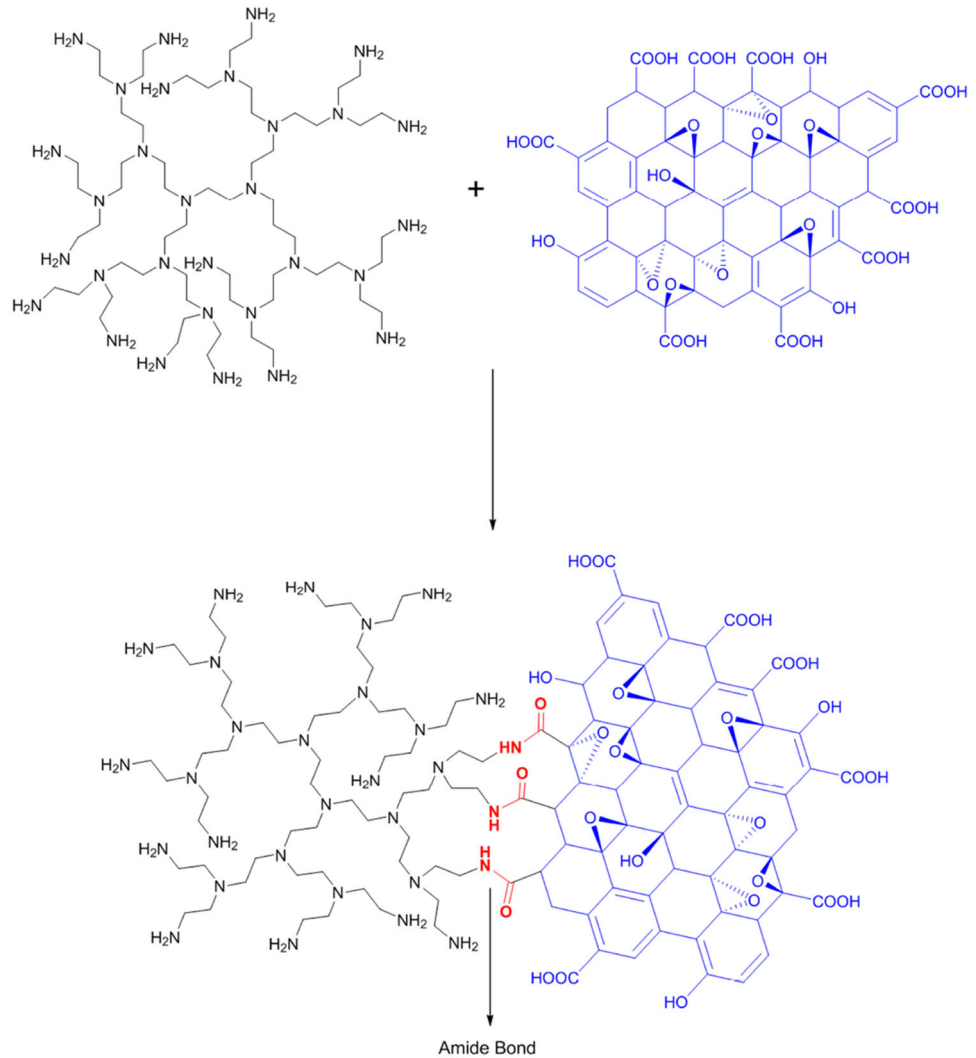
2.4 Instrumentation

The electrochemical experiments were performed with an IVIUM CompactStat electrochemical potentiostat/galvanostat workstation (Ivium Technologies B.V., Netherland). All the experiments were carried out with a three-electrode system with a GCE ($\Phi = 3$ mm) as the commonly used working electrode, a platinum wire as the auxiliary electrode, and an Ag/AgCl/3.0 M KCl as the reference electrode. All the potentials mentioned are referred to this electrode. The electro-analysis was carried out chemically in 0.1 mM PBS solution containing *o*-NP as reference material. The electrolyte was de-aerated with high purity of nitrogen for 15 min previously. All measurements and estimations were performed in a 5-mL of electrochemical cell and all the experiments were carried out at ambient temperature ($25 \pm 0.1^\circ\text{C}$). The GO-PEI was



Scheme 1 Formation of dimanganese heptoxide (Mn_2O_7) from KMnO_4 in the presence of strong acid

Scheme 2 Synthesis scheme for the preparation of GO-PEI dendrimer



electrochemically characterized using cyclic voltammetry (CV) and square wave voltammetry (SWV) in PBS and $[\text{Fe}(\text{CN})_6]^{3-/4-}$ electrolytes. Different concentrations (5–155 μM) of *o*-NP were then prepared, and their SWV were used to plot the calibration curve and to calculate the detection limit.

UV-Vis spectra were obtained using GBC UV/Vis 920 spectrophotometer (GBC Scientific Instruments, Australia), and the sample solutions were prepared by dissolving the materials in distilled water. Raman spectra were measured by PerkinElmer Raman Micro 200 spectrophotometer with a 514-nm laser and 100 \times objective lenses mounted on an

Olympus optical microscope. The laser spot size was taken as 1 μm , and the power on the sample was maintained below 10 mW so as to avoid laser-induced heating, and the spectra were measured in the range of 500–3500 cm^{-1} . All samples were deposited on the glass slides without the use of any solvent. The changes in the functional groups were examined by using an ATR-FTIR spectrophotometer (PerkinElmer, spectrum 100 spectrophotometer) with an accumulation of 16 scans and a resolution of 4 cm^{-1} in the range of 4000–550 cm^{-1} . The scanning electron microscopy (SEM) images for the powdered samples were taken on FEI QUANTA 250 ESEM with an Integrated OXFORD

SIGHT EDS System at 15.00 kV. The transmission electron microscopy (TEM) images were collected on Philips CM10 electron microscope at an accelerating voltage of 100 kV, and the sample was prepared by using distilled water as the dispersing medium and drop-casted onto a carbon-coated copper grid. FAAS measurements were taken with a Model GBC-932-Plus flame atomic absorption spectrometer (GBC Scientific, Australia).

3 Results and discussion

3.1 Physical characterization of GO–PEI composite

UV–Vis absorption spectroscopy confirms about the formation of GO–PEI. The electronic absorption spectra of GO, PEI and GO–PEI were recorded in the range of 450–200 nm with a 1-cm quartz cell path and are shown in Fig. 3a. From the figure, the peaks were observed in the middle ultraviolet region of 350–200 nm. A 3-mL volume

of each sample was analysed separately at room temperature with their wavelengths having a maximum absorption at 230 and 295 nm for GO, 292 nm for PEI and 263 and 350 nm for GO–PEI, respectively. Figure 3a shows that GO maintains carboxyl and hydroxyl functional groups on the edges of their basal planes. Thus, GO shows the π – π^* transitions of an aromatic C=C bonds at 230 nm [20], whereas the shoulder n – π^* transitions of carboxylic acid group's C=O bonds at 295 nm [21]. With respect to it, there is not even an absorption peak corresponding to the GO in the UV–Vis spectra. It is well known that, as reduction proceeds, the size of electronically conjugated domains increases and the absorption peak position gradually changes to red-shift, which can thus be considered to a first approximation, as an indication of the reduction degree attainment [22]. Among the entire peak formed, the absorption spectrum of GO–PEI is of high significance, i.e. the absorption peaks found to appear at 263 and 350 nm due to the restoration of π electron conjugation within the graphene sheets [23]. This shift in peak position provides evidence for the reduction of surface functional groups on the GO sheets which has been recorded. The PEI shows that the curve is in continuous decreasing pattern, and there is no peak formed around 300–350 nm in Fig. 3b, which suggests the reduction of GO and the recovery of conjugate structures. Further, the absorption spectra were analysed by fitting to the Gaussian function [24, 25], and the results of the Gaussian analysis for all systems under study are shown in Table 1.

All the samples were analysed by Raman spectroscopy because of the unusual band broadening and the shifts of Raman bands with decreasing particle size. However, there is no general agreement and strategy about the origin of broadening and shifts of Raman bands. By the Heisenberg uncertainty principle, the relationship between particle size and phonon position can be expressed as follows:

$$\Delta X \cdot \Delta P \geq \frac{\hbar^2}{4} \quad (1)$$

where ΔX is the particle size, ΔP is the phonon momentum distribution, and \hbar is the reduced Planck's constant, respectively. As the particle size decreases, the phonon is increasingly confined within the particle, and the phonon momentum distribution also increases. This broadening of phonon momentum finally leads to the broadening of scattered phonon momentum as stated in the law of conservation of momentum. This phonon dispersion causes, in general, the asymmetric broadening and may lead to a shift in the Raman bands [26]. The Raman spectroscopy is a powerful tool to measure the phonons in the Brillouin zone centre, which possess strong selection rules and is known to be a powerful technique for the investigation of even subtle structural distortions and ferroelectric polarizations.

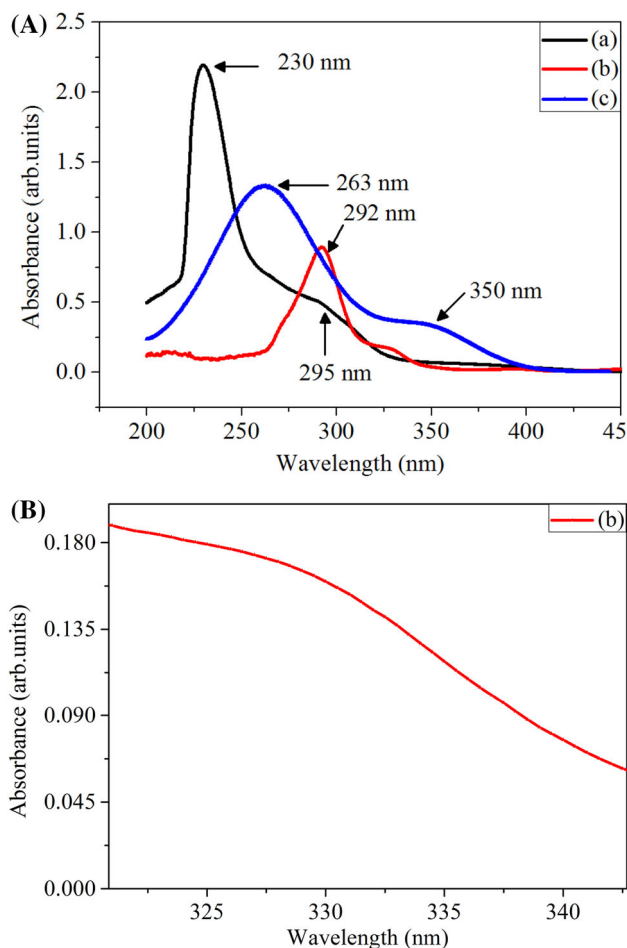


Fig. 3 a Comparison of the UV–Vis absorption spectroscopic images of a GO b PEI, and c GO–PEI. b Absorption spectrum of PEI around 300–350 nm

Table 1 Gaussian curve analysis for the bands in spectrum of all samples at 25°C

System	Area of the curve (A)	Width of the curve (w)	Centre of the curve (x_c)	y_0	R^2
GO	71.756 ± 1.489	32.750 ± 0.721	234.625 ± 0.335	0.119 ± 0.009	0.867
PEI	25.429 ± 0.309	26.715 ± 0.344	290.683 ± 0.164	0.057 ± 0.002	0.949
GO–PEI	82.295 ± 0.823	61.971 ± 0.50	264.420 ± 0.209	0.123 ± 0.004	0.953

More details of the structural evolution with GO–PEI can be expressed through Raman spectra. The measured Raman scattering spectra of GO, PEI, and GO–PEI samples at room temperature are shown in Fig. 4. It is well known that GO yields four Raman-active modes with distorted hexagonal structure and is summarized using the irreducible representation [27].

$$\Gamma_{\text{RAMAN}} = A_{2u} + B_{2g} + E_{1u} + E_{2g}$$

where A_{2u} and E_{1u} representations are the translations of the plane; the B_{2g} mode is an optical phonon where the carbon atoms move perpendicular to the graphene planes. E_{2g} is the doubly degenerate in-plane optical vibration. It was found that only the E_{2g} representation is Raman active. The Raman

spectroscopy of GO is characterized by two main features: the G-peak, which arises from the first-order scattering of the E_{2g} phonon from sp^2 carbon atoms from the aromatic structure which is observed at 1575 cm^{-1} , and the D-peak at 1355 cm^{-1} that arises from breathing mode of κ -point phonons of A_{1g} symmetry from sp^3 carbon atoms of the defect structure [28]. In our system of experimentation, the Raman spectrum of GO shows the characteristic G band at 1583 cm^{-1} and D band at 1366 cm^{-1} , respectively. The former one is due to the vibration of sp^2 bonded carbon atoms in a 2D hexagonal lattice [29], and the latter is caused by the vibrations of carbon atoms with dangling bonds in the plane of terminations of disordered graphite [30]. The second-order Raman feature, namely the 2D band at 2700 cm^{-1} , is very sensitive as well as effective to the stacking order of graphene sheets along the c -axis and also to the number of layers [31]. It reveals that the prepared GO was pure to large extend. PEI shows a band at 1383 cm^{-1} corresponding to the C–H deformation, and the band in the region of 1533 cm^{-1} is due to the N–H stretching. GO–PEI shows that the G bands are shifted to 1575 cm^{-1} , suggesting the reduction of GO by PEI [32]. The D band showed slight deflection at 1390 cm^{-1} , which is correlated with structural defects. The intensity ratio (I_D/I_G) of the D band (I_D) and the G band (I_G) signifies the amount of defect and disorder structure. The intensity ratio increases from 0.86 for GO to 0.88 for GO–PEI, showing the reduction of oxygen functional groups and the conversion of sp^3 carbon of GO to sp^2 carbon in GO. The increased intensity of the D band of GO–PEI planar sheets indicates the presence of sp^3 defects within the sp^2 carbon network of graphene [33], resulting in the nucleophilic addition of $-\text{NH}_2$ functionalities of PEI to the epoxy functionality of GO and the covalent bond formed during the reduction process [34]. Thus, the analysis of FTIR and Raman confirms for the successful synthesis of GO–PEI composite.

The presence of functional groups in the samples was confirmed by the FTIR spectra in Fig. 5. GO is specifically a graphene sheet with carboxylic groups at its edges and phenol hydroxyl along with epoxide groups on its basal plane [35]. For GO (Fig. 5a), the peak appeared at 3025 cm^{-1} can be attributed to the O–H stretching vibrations of adsorbed water molecules and structural O–H groups, and the peak appeared at 1595 cm^{-1} can be attributed to O–H bending vibrations which are highly

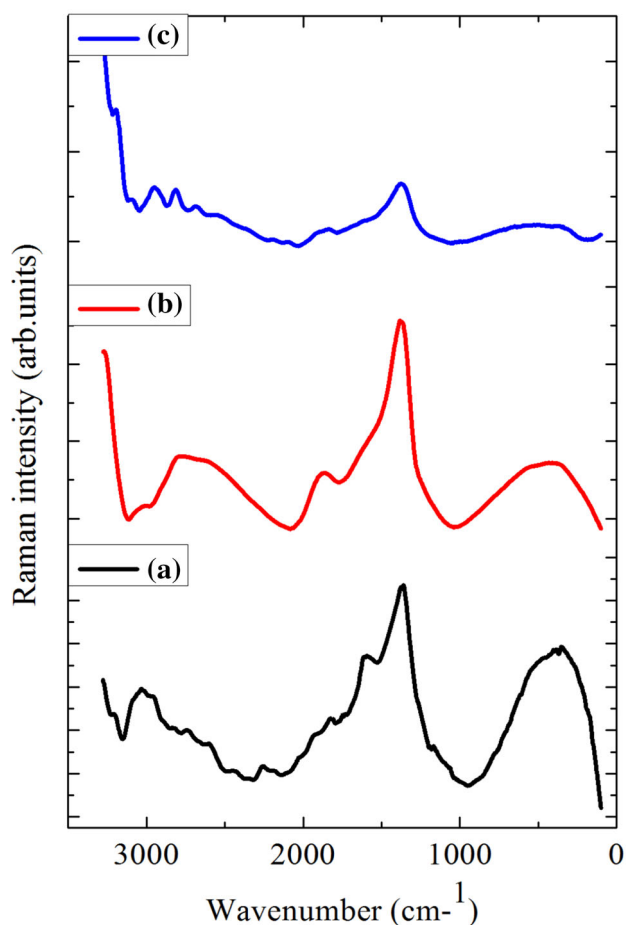


Fig. 4 Comparison of the Raman spectra of *a* GO *b* PEI, and *c* GO–PEI

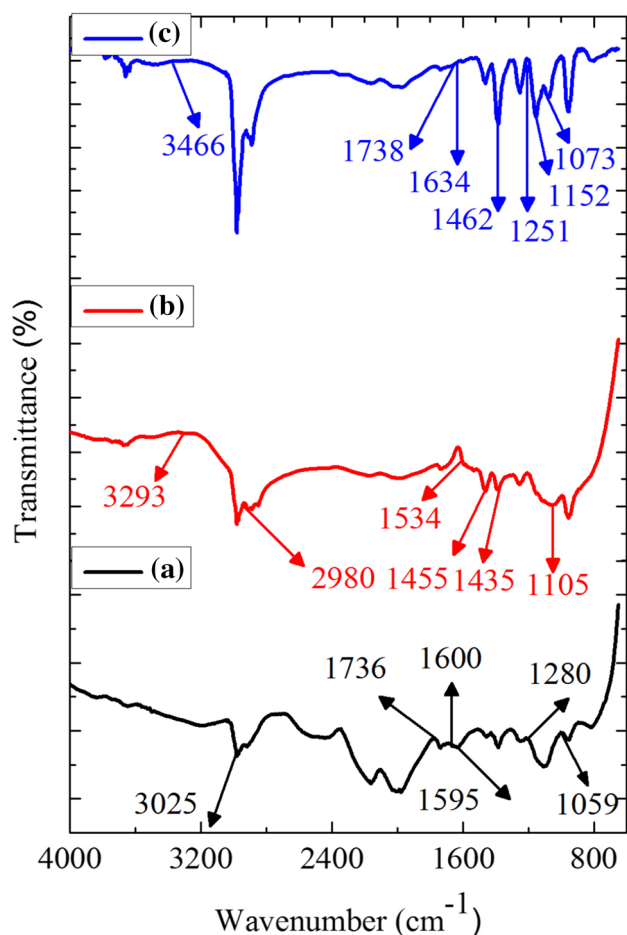


Fig. 5 Comparison of the FTIR spectra of *a* GO *b* PEI *c* GO-PEI

confined to each other. The presence of carboxyl and epoxy functional groups can also be detected at around 1736 and 1280 cm^{-1} , 1059 cm^{-1} , respectively [36]. The above evidence indicates that during the oxidation process of the graphite powder with KMnO_4 in the presence of concentrated H_2SO_4 , the original extended conjugated π -orbital system of the graphite was destroyed and the oxygen-containing functional groups were inserted into the carbon skeleton which is of great significance. The peak at 1600 cm^{-1} is arising from C=C skeletal vibrations from unoxidized graphitic domains [37]. It was also observed that the C–O stretching mixed with phenolic hydroxyl group C–OH bending at 1050 cm^{-1} and O–H–O out of plane wagging at 800 cm^{-1} [38]. The FTIR spectrum of PEI (Fig. 5b) illustrates the peaks corresponding to amine N–H stretching at 3293 cm^{-1} , and the amine N–H is bending at 1534 cm^{-1} , methylene stretching at 2980 cm^{-1} , and methylene bending at 1435 cm^{-1} . One characteristic band for CH_2 had appeared around 1455 cm^{-1} for the bending vibrations, and similarly, the band corresponding to stretching mode of C–N bond appeared at 1105 cm^{-1} . On the other hand, the FTIR spectrum of GO-PEI (Fig. 5c)

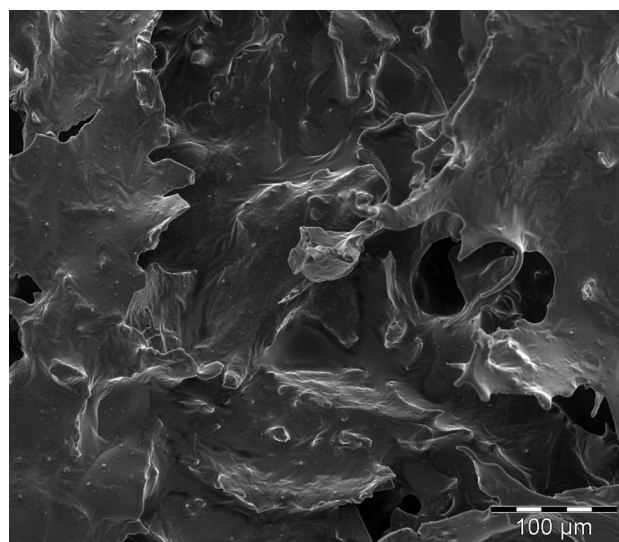


Fig. 6 SEM image of GO-PEI

exhibits significant alterations as compared to those of individual structures. For instance, it was found to be carboxyl group at 1738 and 1251 cm^{-1} , epoxy group at 1073 cm^{-1} , CH_2 at 1462 cm^{-1} , and C–N at 1152 cm^{-1} . The major difference between this spectrum and the others is the specific appearance of a new group frequency at 3466 and 1634 cm^{-1} which is related to the amide N–H group significantly [39, 40]. This result provides a supporting evidence for the successful covalent reaction that has taken place between GO and PEI. Such a peak does not appear in the spectra of simple GO or PEI.

Figure 6 shows the SEM image of GO-PEI. It reveals that it is a porous structure with a large number of adsorption sites. It is also observed that the surface of GO sheets is smooth and tightly packed owing to the interaction of oxygen-containing functional groups [41].

Figure 7 shows TEM image of GO-PEI formed by the surrounding of PEI chain with the GO, through electrostatic interaction, the covalent bond between the PEI chain and GO. Such formation of GO-PEI is mainly due to low grafting density of PEI chain and weak bond linkage between PEI and GO. The colour of the particular composite darkens in TEM images states the attachment of more PEI chain on GO where the size of particle ranges in the region around is 200 nm (scale).

3.2 Optimization of experimental parameters for the determination of GO-PEI

3.2.1 Effect of GO-PEI concentration

Table 2 shows the influence along with the enhancement of concentration of GO-PEI suspension on the reduction peak

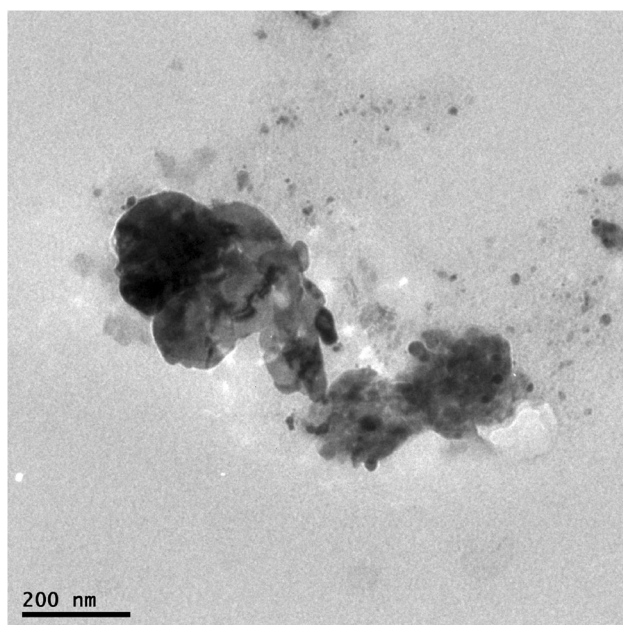


Fig. 7 TEM image of GO-PEI

Table 2 Various combination ratios of the samples prepared

Samples	Mixing volume ratio		Current peak (μA)
	GO (mL)	PEI (mL)	
S-1	0.25	1.75	-102.12
S-2	0.50	1.50	-102.46
S-3	0.75	1.25	-102.58
S-4	1.00	1.00	-103.93
S-5	1.25	0.75	-103.57
S-6	1.50	0.50	-102.98
S-7	1.75	0.25	-102.67

current. From the table, a gradual improvement in the content of GO-PEI suspension seems to enhance the peak current of GO-PEI. While with an increase in the content of GO-PEI suspension from 0.25 to 1 mL, the effective surface area and the accumulation efficiency is also improved accordingly. Consequently, as a result, the surface concentration of GO-PEI increases, and then, the reduction peak current also enhances. With further increase in the content from 1 to 1.75 mL, the reduction peak current of GO-PEI decreased slightly, suggesting that if the modified GO/PEI is too thick, it is not beneficial for the sensing. The GO-PEI was prepared by mixing GO with that of PEI in different proportions as listed in Table 2. In this process of experimentation, the sample number 4 (S-4) was selected for detailed studies by its different properties such as high reduction peak current, reproducible behaviour, and mechanical stability as compared to the other samples.

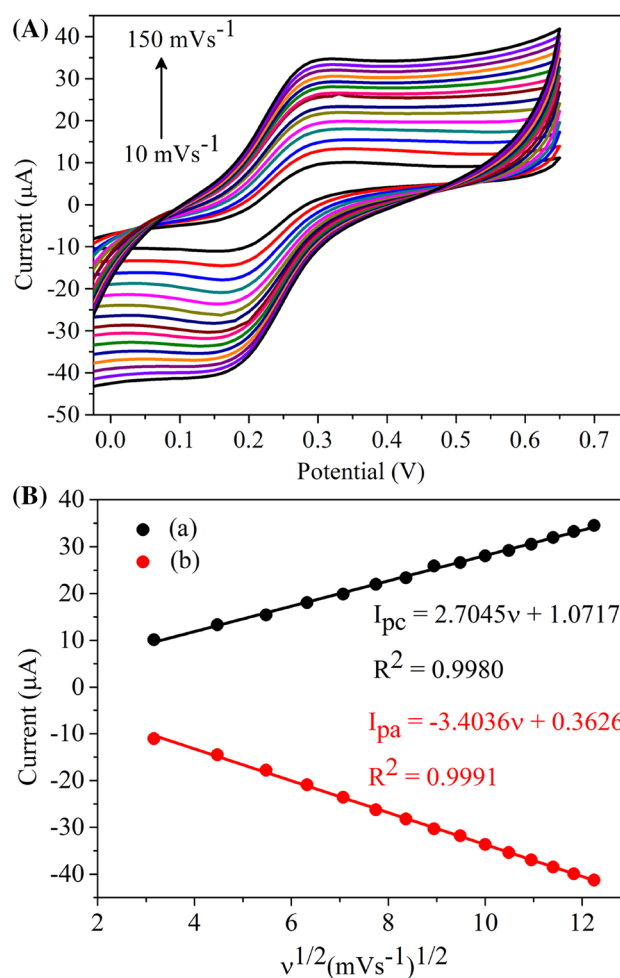


Fig. 8 **a** Comparison of the CVs of GO-PEI at different scan rates with 5 mM $[\text{Fe}(\text{CN})_6]^{3-/4-}$ at pH 5. **b** Relationship between the I_{pc} and I_{pa} values and the square root of scan rate

3.2.2 Effect of scan rate

Following the physical characterization, the surface layer was evaluated and found that the surface obtained after the modification on bare GCE is more suitable for different applications. Further, the composite was analysed to see whether it supports genuinely for the binding of electrode surface diffusion controlled or not. Some useful information related to electrochemical mechanism usually can be acquired from the relationship between the peak current and scan rate. The CV technique can be employed for testing the barrier kinetics of the catalytic interface with the electro-active species $[\text{Fe}(\text{CN})_6]^{3-/4-}$ (FCN). Also, the kinetic hindrance to the electron transfer process increases in general with an increase in material thickness and tends to decrease with the defect density of the barrier. The CV studies for the GO-PEI composite in 5 mM $[\text{Fe}(\text{CN})_6]^{3-/4-}$ buffer solution as a function of the effect of scan rate and peak current are shown in Fig. 8a, b. From the figure, the

peak current seems to be increased gradually with an increase in scan rate because of the influence of voltage on the current for every reversible electron transfer regarding the diffusion layer thickness. When the study was done at a high scan rate, the anodic potential shifted more gently towards the positive potential, whereas the cathodic peak potential is in reverse direction. The anodic and cathodic peak currents are found to increase in straight form with an increase in scan rates, representing the limits of diffusion control. Hence, it is inferred that the peak currents are proportional to the square root of the scan rate. When the scan rate is inserted in the range of 10–150 mVs^{-1} , the expression derived is as follows: $I_{\text{pc}} (\mu\text{A}) = 2.7045 v (\text{mVs}^{-1}) + 1.0717 (R^2 = 0.9980)$ and $I_{\text{pa}} (\mu\text{A}) = -3.4036 v (\text{mVs}^{-1}) + 0.3626 (R^2 = 0.9991)$. The ratio of anodic peak current to the cathodic peak current is almost equal to unity. It was shown that the oxidation and reduction on GO-PEI is a diffusion-controlled process. Consequently, it can be used for pre-concentration micro-quantity onto the surface of GO-PEI synthetically for quantitative analysis. The scan rate was chosen as 50 mVs^{-1} in order to increase and decrease the background currents and also for obtaining the high sensitivity for further experiments to be carried on.

3.2.3 Electrochemical characterization of GO-PEI

CV experiments were performed using 5 mM $[\text{Fe}(\text{CN})_6]^{3-/4-}$ buffer solution containing 0.1 M KCl at 50 mVs^{-1} scan rate. Figure 9 represents the representative CVs of (a) bare GCE, and (b) GO-PEI. From the figure, a pair of well-defined redox peaks are observed at the GCE with the cathodic peak potential E_{pc} at 0.274 V, the anodic peak

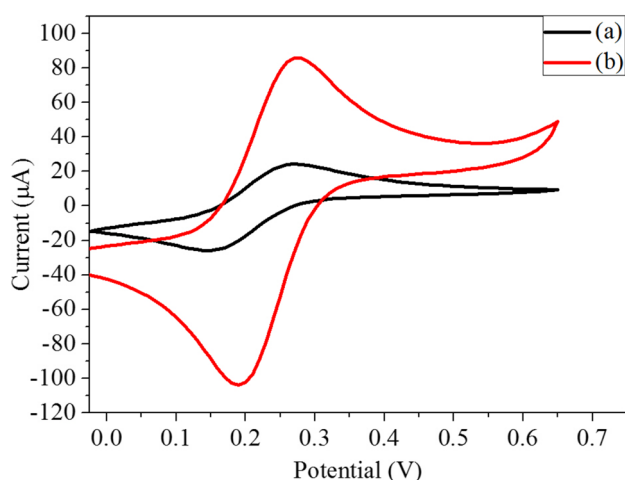


Fig. 9 Comparison of the CV of a bare GCE, and b GO-PEI in with 5 mM $[\text{Fe}(\text{CN})_6]^{3-/4-}$ (1:1) solution containing 0.1 M KCl. The scan rate of CV is 50 mVs^{-1} at pH 5

potential E_{pa} at 0.148 V, respectively, and peak-to-peak separation ΔE_p of 0.126 V, indicating that the electrode process of $[\text{Fe}(\text{CN})_6]^{3-/4-}$ is reversible. The GO-PEI shows a good replica as compared to bare GCE with the cathodic peak potential of 0.282 V and anodic peak of 0.194 V and peak-to-peak separation (ΔE_p) of 0.088 V resembling less sensitivity. The higher redox peak currents are obtained at the GO-PEI, possessing that the electrochemical active site of GCE is increased with the modification in GO-PEI surface, resulting from the excellent conductivity ability and large surface area of GO-PEI. As soon as the electrode is coated with GO-PEI, the redox peak current decreases, which reveals that there is a negatively charged carboxyl group on the GO surface [42]. The peak separation is reversible electron transfer reaction, indicating that the process is quasi-reversible between $\text{Fe}(\text{CN})_6^{4-}/\text{Fe}(\text{CN})_6^{3-}$ couple and the electrodes. It is clear from the above facts that GO has been successfully assembled on the electrode surface and provided a specific conduction pathway for promoting the electron transfer between the analyte (ferri cyanide) and the electrode surface. The passivation of the electrode surface is illustrated by a decrease in the peak height and the higher-conductivity PEI acts as an electron transfer channel, later on playing a significant role in improving the conductivity of GO. The GO-PEI improves the reversibility of the electrode reaction process and the electrochemical enhancement of both anodic and cathodic peak current. The GO-PEI is modified on the GC electrode surface excavated due to an increase in the current.

3.3 Cyclic voltammetry of o-NP

3.3.1 Electrochemical characterization of the presence and absence of o-NP at GO-PEI

The o-NP can be easily identified by the electrochemical methods, and in most of the electrolytes, the optimum pH for the electro-reduction of NP lies in the range of 4–7 [43]. Figure 10 shows the CV of GO-PEI in the absence and presence of 5 mM o-NP at 50 mVs^{-1} . From the figure, no redox peaks are observed at GO-PEI in the absence of 5 mM o-NP because of the electro-inactive behaviour in the selected potential region. In the presence of GO-PEI, the CV for 5 mM o-NP on the anodic peak at 0.35 V and cathodic peak potential at 0.15 V and peak-to-peak separation ΔE_p of 0.2 V were observed, meaning that the GO-PEI exhibited excellent improvement in current signals towards o-NP. The enhancement of peak current at the GO-PEI was mainly due to the complexation reaction formed in the experimentation process. The reduction peak current increases to a higher level as compared to the oxidation peak current, and also the reduction peak potential was found to be a positive shift. The catalytic

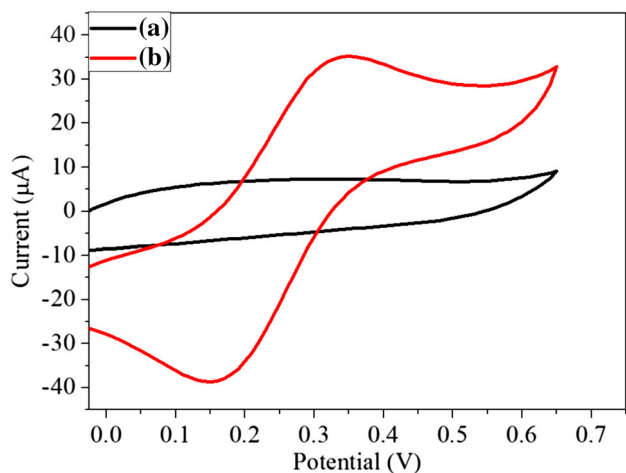
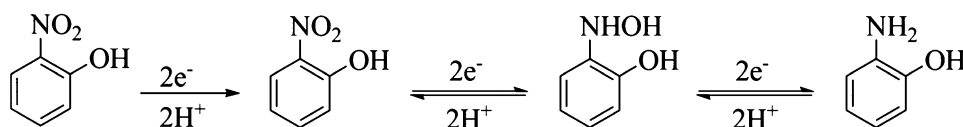


Fig. 10 Comparison of the CVs of GO-PEI *a* in the absence and *b* in the presence of 5 mM *o*-NP in 0.1 mol L⁻¹ PBS solution. The scan rate of CV is 50 mVs⁻¹ at pH 5

effects noticed at the GO-PEI show the following synergistic effect mainly due to the presence of *o*-NP. They are as mentioned: (a) free radicals in GO were observed, (b) GO was found to have superior conductivity and includes large surface area, and (c) π - π stacking between GO and *o*-NP was found due to an aromatic structure of *o*-NP. The reduction peak potential is found higher than at single-wall carbon nanotube-coated electrode (0.72 V, vs. SCE) [44], multi-wall carbon nanotubes Nafion-modified electrode (-1.0 V, vs. SCE) [45], and lithium tetracyanoethylene-modified electrode (0.70 V, vs. Ag/AgCl) [46] in aiding the conditions in an adequate manner. Thus, the GO-PEI formed investigated to be highly sensitive for the detection of *o*-NP. Therefore, a substantial decrease in the reduction over potential has been achieved to a large extent in the present study with GO-PEI, and the reduction peak current can be chosen as an analytical signal to detect the *o*-NP.

3.3.2 Electrochemical reduction process of *o*-NP at GO-PEI

Figure 10 shows the two peaks obtained from the CV of *o*-NP, and the corresponding reaction mechanism is shown in Scheme 3. In the reaction, *o*-NP gets electrochemically reduced to aminophenol standing by an ECE mechanism. The cathodic peak found at 0.35 V is mainly due to the



Scheme 3 Schematic of the possible reduction mechanism of *o*-NP into aminophenol at GO-PEI

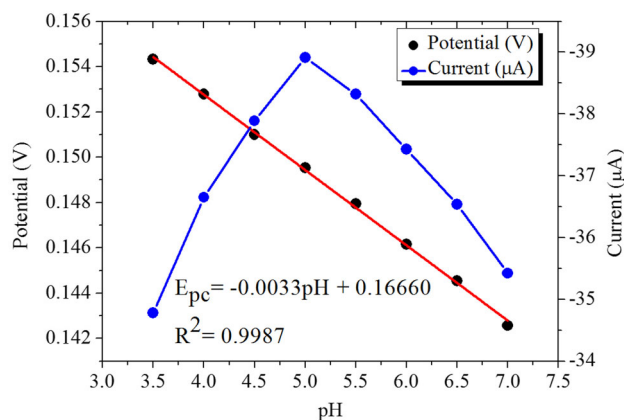


Fig. 11 Cathodic peak potential as a function of 5 mM *o*-NP in 0.1 mol L⁻¹ PBS solution. Scan rate of CV is 50 mVs⁻¹

irreversible oxidation of hydroxyl group [47], whereas the redox couple at +0.15 V is because of the reversible two-electron oxidation–reduction of the *o*-hydroxylamine group (-NHOH) to a nitroso group (-NO). The reduction of nitro group of *o*-NP occurs through an intermediate product hydroxyl aminophenol and an irreversible $4e^-/4H^+$ electrochemical reduction reaction. When the water molecule is removed from the intermediate product, it converts into benzoquinoneimine, which further gets reduced to aminophenol by an equilibrium process [48].

3.3.3 Effect of the pH of *o*-NP at GO-PEI

In general, the electrochemical system randomly gets influenced by the changes in pH values, as there is an active involvement of the protons in an overall electrode reaction. In that way, there is a possibility for GO-PEI to show a significant change in the CV response close to the solution pH. Figure 11 shows the changes in the peak current/potential for the GO-PEI in the range of 3.5–7. From the figure, it appears that there is an increase in the peak current/potential during the pH range of 3.5–5, and the maximum current is seen for the pH of 5. However, with further increase in pH, the peak current observed to be decreased. This phenomenon can be attributed to two conditions: (1) the presence of proton is critical during the redox behaviour of *o*-NP and (2) the decrease in *o*-NP response at high pH is mainly due to the decrease in proton concentration. Hence, pH 5 was considered as the best one,

and it was selected as the optimum pH for the analytical experiments. It was later on found that with a further increase in solution pH, the protonation, an essential step for the reduction of *o*-NP, also tends to decrease. The relationship between the reduction peak potential and pH is shown in Fig. 11. With an increase in solution pH from 3.5 to 7.0, the E_{pc} shifted to a negative value and the linear equation is shown below.

$$E_{pc}(V) = -0.0033\text{pH} + 0.1666, (R^2 = 0.9987).$$

According to Eq. (2) [49]:

$$\frac{dE_p}{dpH} = -2.303 \frac{mRT}{nF} \quad (2)$$

where m and n correspond to the number of protons and electrons transferred. The value of m/n was calculated as 1.02 approximately equal to 1.0, referring that the number of protons transferred was same as a number of the electrons. The results revealed that the *o*-NP is getting reduced to hydroxyl aminophenol with a transfer of two electrons and two protons, and this result was also consistent with the above analysis.

3.3.4 Effect of scan rate of *o*-NP at GO-PEI

The effect of scan rate of *o*-NP at GO-PEI observed during the investigation is shown in Fig. 12a–b. From the figure, it appears that both the oxidation and reduction peaks are enhanced with an increase in scan rate, while the peak potential remained almost unchanged which was noticed during the experimental process. The peak currents are found to increase with an increase in scan rate which is attributed to fit for the electrodes. Later, it was noticed that the peak potential was found to be altered a little with an increase in scan rate. All such factors indicate that at higher scan rates, the redox reaction is found to be quasi-reversible. The reduction and oxidation peak currents of *o*-NP show that they are linearly proportional to the square root of scan rate in the range of 10–150 mVs^{-1} . The linear regression equation was as follows: $I_{pa}(\mu\text{A}) = -4.8993 v(\text{mVs}^{-1}) - 3.8932$ ($R^2 = 0.9972$) and $I_{pc}(\mu\text{A}) = 4.0578 v(\text{mVs}^{-1}) + 5.5874$ ($R^2 = 0.9987$). The ratio of anodic peak current to cathodic peak current is approximately equal to unity, which resembles that the electrode process of *o*-NP at GO-PEI was controlled by diffusion.

3.3.5 Detection limit of different concentrations of *o*-NP at GO-PEI

SWV of GO-PEI recorded with 5 mM $[\text{Fe}(\text{CN})_6]^{3-/4-}$ solution containing *o*-NP at concentrations in the range of 5–155 μM is shown in Fig. 13a–b. Figure 13a shows that there is an increase in the current with an increase in the

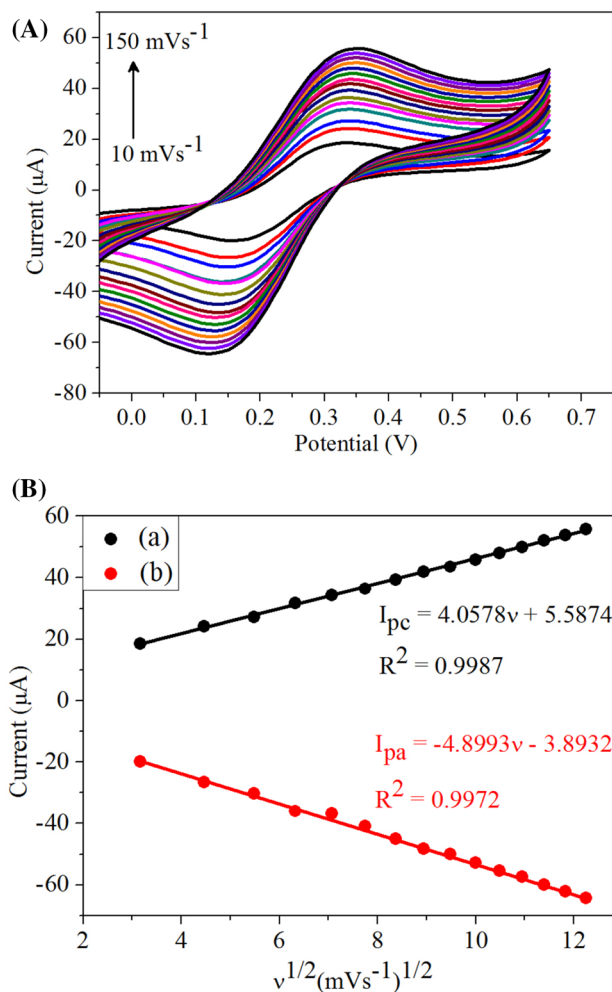


Fig. 12 a CV of *o*-NP at GO-PEI at different scan rates with a concentration of 5 Mm at pH 5. b The relationship between current peak and square root of scan rate

concentration of *o*-NP. We observed only a single reduction peak at high or low concentration of *o*-NP. The plot of current versus different concentrations in the range of 5–155 μM is shown in Fig. 13b, a linear increase in current with respect to an increase in the concentration of *o*-NP can be seen. These results indicate that the GO-PEI is an appropriate electrode material for studying the electrochemical reduction behaviour of *o*-NP. The calibration plot as designated shows a linear relationship with a correlation coefficient which obeys the equation apparently.

$$I_{pa}(\mu\text{A}) = 0.0159C(\mu\text{M}) - 15.1447, (R^2 = 0.9963)$$

The detection limit was calculated using the formula given in Eq. (3):

$$\text{D.L} = \frac{3.3 \times \sigma}{\text{slope}} \quad (3)$$

where σ is the standard deviation of blank which was taken three times so as to eliminate the error. The detection limit was

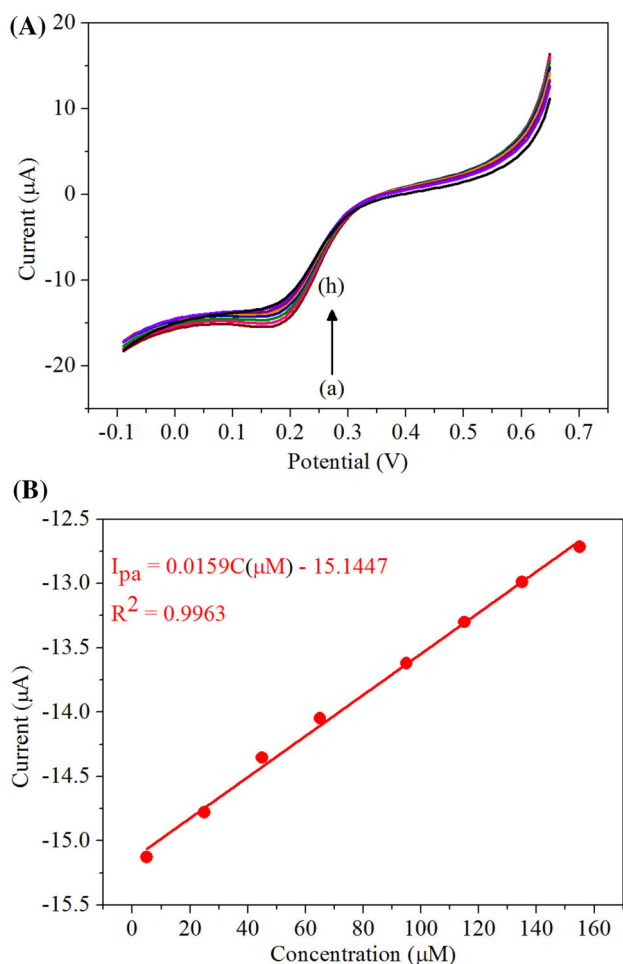


Fig. 13 **a** SWV of GO-PEI electrode recorded with a sweep rate of 50 mVs^{-1} in $5 \text{ mM } [\text{Fe}(\text{CN})_6]^{3-/4-}$ at pH 5 using *a* $5 \mu\text{M}$, *b* $25 \mu\text{M}$, *c* $45 \mu\text{M}$, *d* $65 \mu\text{M}$, *e* $95 \mu\text{M}$, *f* $115 \mu\text{M}$, *g* $135 \mu\text{M}$, and *h* $155 \mu\text{M}$ of *o*-NP. **b** The relationship between peak current and different concentrations of *o*-NP

found to be $0.1 \mu\text{M}$, under the optimized conditions, and the concentration produced a signal-to-noise (S/N) ratio of 3.

Different types of modified electrodes have been reported in the past for simultaneous determination of *o*-

NP. The performances of modified electrodes and the electrode prepared in our study are listed in Table 3. Among the various electrodes, the GO-PEI showed the lowest detection limit for *o*-NP as $0.1 \mu\text{M}$. The result of the study therefore indicates that the GO-PEI-modified electrode can be suitable for the detection of *o*-NP using an electrochemical technique.

3.3.6 Repeatability and stability of *o*-NP at GO-PEI

The experiment from fresh bare GCE was repeated thrice, and from the observation of closer results, it can be conferred that the electrode showed a good reproducibility. For the diluted concentration of $155 \mu\text{M}$, the peak current was noticed to be $-12.71 \mu\text{A} \pm 1.52 \times 10^{-8}$ with a relative standard deviation of 0.12 %, suggesting the acceptable reproducibility and precision capability. The limitation was taken as ten for the number of measurements carried out with the same electrode so as to avoid the loss of initial signal occurred due to the desorption of *o*-NP. As such, the electrode's surface was cleaned. A new electrode was prepared after ten measurements.

The GO-PEI electrode was stored for about three months in a refrigerator at 4°C . Meanwhile, some new electrodes were prepared by employing the same procedure. Figure 14 shows the results of the measurement of the current response of the same electrode carried out after 15-day intervals examination of the stability of GO-PEI sensor for an extended period. The results show that the current response to *o*-NP decreases to 99.97 % even after 15 days, but the original current response continued as 96.72 % after 60 days, and the current response to *o*-NP decreases to 99.97 % even after 15 days. It also shows that electrode absorbed 95 % of its original response after 90 days as well. Thus, the difference in the peak currents such as the analytical response of *o*-NP reduction from each new electrode prepared was less than 5 %, reflecting the good stability of GO-PEI/GCE sensor.

Table 3 Comparison of the analytical performance of different chemically modified electrodes for the determination of *o*-NP with GO-PEI-modified electrode

Modified electrode	Method	Linear range (μM)	Detection limit(μM)	References
Nano-Au ^a /GCE	SDV	50–1000	8	[50]
CD-RGO ^b /GCE	DPV	7.0–64	0.14	[51]
CNTs ^c /GCE	LSV	2.0–400	0.5	[52]
GR-CS ^d /GCE	LSV	1–240	0.2	[53]
GO-PEI/GCE	SWV	5–155	0.10	This work

^a Nano-Au, nanogold

^b CD-RGO, β -CD functionalized reduced graphene oxide

^c CNTs, carbon nanotubes

^d GR-CS, graphene-chitosan composite

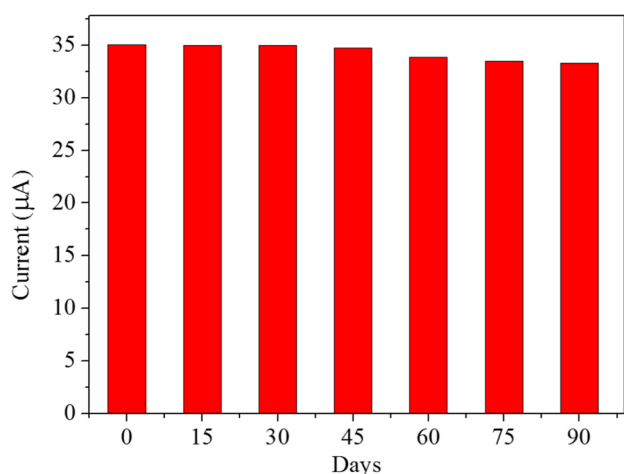


Fig. 14 Peak currents of GO-PEI measured every 15 days in 5 mM *o*-NP at pH 5

3.4 Analysis of environmental samples using columns of GO-PEI by FAAS

Various samples were collected from different industrial areas of Aligarh City, India, and were filtered through millipore cellulose membrane filter (0.45- μ m pore size), acidified with concentrated HNO₃, and finally subjected to the recommended procedure (column operation) mentioned

below for pre-concentration. In the pre-concentration procedure, a sample pH of around 5.0–6.0 was adjusted to approximately 6.0 with acid and passed through the material at a minimum rate of 5 mL min⁻¹. The adsorbed metal ions were then eluted with 5 mL of 2 M nitric acid in acetone at a flow rate of 1 mL min⁻¹. After that, by making use of the FAAS, the total amount of metal ion contents in the eluent was determined.

The practical utility of the material was demonstrated by the analysis of metal ions from environmental samples as given in Table 4. The validity of the method was checked by performing five replicate analyses of the samples. Therefore, the method seems to be precise and accurate which is evidential according to the standard deviation data.

4 Conclusion

In conclusion, we report a low-cost, sensitive, and accurate probe for the electrochemical detection of volatile organic pollutants in the environmental samples. For that, we prepared the GO-PEI composite and studied its electrochemical behaviour towards the detection of *o*-NP by comparing its efficiency against bare GCE. The prepared composite was thoroughly investigated by the use of

Table 4 Analysis of Fe³⁺, Ni²⁺, Cu²⁺, Pb²⁺, and Zn²⁺ ions by the use of GO-PEI composite material

Samples	Method	Amount of Fe ³⁺ found* (ppb) (% RSD) ^a	Amount of Ni ²⁺ found* (ppb) (% RSD) ^a	Amount of Cu ²⁺ found* (ppb) (%RSD) ^a	Amount of Pb ²⁺ found* (ppb) (% RSD) ^a	Amount of Zn ²⁺ found* (ppb) (%RSD) ^a
1	Direct ^b	84.1 (3.6)	1324 (4.1)	6.2 (2.2)	11.5 (0.11)	569 (2.0)
	SA ^c	84.9 (4.4)	1325 (2.5)	7.0 (2.5)	12.8 (2.5)	570 (3.2)
2	Direct ^b	687 (1.6)	2812 (2.3)	0.3 (3.1)	14.8 (0.14)	577 (1.82)
	SA ^c	688 (0.29)	2813 (1.0)	0.6 (2.8)	15.0 (3.4)	5779 (1.3)
3	Direct ^b	32.5 (1.9)	3887 (1.8)	6.8 (1.2)	0.7 (0.7)	339 (1.4)
	SA ^c	33.0 (3.2)	3888 (1.6)	7.0 (0.21)	0.9 (2.3)	340 (4.7)
4	Direct ^b	357.8 (2.2)	13174 (3.2)	0.30 (1.8)	6.9 (0.69)	2157 (1.5)
	SA ^c	359 (4.5)	13176 (3.4)	0.35 (3.3)	7.1 (1.5)	2158 (0.8)
5	Direct ^b	245 (2.7)	3288 (2.2)	4 (3.4)	19 (1.8)	818 (1.6)
	SA ^c	246 (1.2)	3289 (2.9)	6 (2.9)	26 (2.6)	820 (0.35)

Experimental conditions: 100 mL solution, sorption flow rate 2.0 mL min⁻¹, 0.5 g material

1 (Aligarh Sasni Area, Aligarh)

2 (Abdul Kareem Area, Aligarh)

3 (C.P. Road, Aligarh)

4 (City Lock and Key Industry, Aligarh)

5 (Talanagri, Aligarh)

^a Relative standard deviation

Direct^b Recommended procedure applied without spiking

SA^c Recommended procedure after spiking (standard addition method)

* Average of three replicates determinations (% RSD)

instrumental analysis that includes UV–Vis, FTIR, Raman, SEM, and TEM. It was evident from an analysis of results that graphene sheets act as a connector for accumulating the active amino groups of PEI providing a sustainable environment for carrying additional functionalization. On testing, the GO–PEI-modified electrode exhibited an enhanced activity towards the volatile *o*-NP using a reduction mechanism of GO by PEI where the epoxy group is diminished by amine groups through the nucleophilic ring-opening reaction, and it was later carried out by an elimination reaction. A broad application of GO–PEI for the sensitive detection of *o*-NP and also for the removal of metal ions in the environmental samples showed its potency to a larger extent. At GO–PEI, the *o*-NP can be identified and separated, and with the CV instrument, the reduction peaks for the *o*-NP are observed at 0.35 V, and this sensitive electrochemical response is investigated to be due to the bonding of PEI onto the GO. By making use of the GO–PEI-modified electrode, a low detection limit of 0.1 μM for *o*-NP was obtained, thereby confirming its applicability for the analysis of real-time industrial samples. In addition, the material also investigated to be active for the removal of essential metal ions (Fe^{3+} , Ni^{2+} , Cu^{2+} , Pb^{2+} , and Zn^{2+} ions) from industrial effluents. Thus, as the composite possesses, physico-chemical properties can be used for the development of novel technologies to play a significant role in the monitoring and management of pollutants from entering into the environment.

Acknowledgments The authors thank University of Johannesburg and Aligarh Muslim University for providing facilities. We thank an anonymous reviewer for constructive criticism on earlier manuscript version.

References

- Wang P, Xiao J, Liao A, Li P, Guo M, Xia Y, Li Z, Hiang X, Huang W (2015) Electrochemical determination of 4-nitrophenol using uniform nanoparticle film electrode of glass carbon fabricated facilely by square wave potential pulses. *Electrochim Acta* 176:448–455. doi:10.1016/j.electacta.2015.07.054
- Isayev O, Rasulev B, Gorb L, Leszczynski J (2006) Structure-toxicity relationships of nitroaromatic compounds. *Mol Divers* 10:233–245. doi:10.1007/s11030-005-9002-4
- Miró M, Cladera A, Estela JM, Cerdá V (2001) Dual wetting-film multi-syringe flow injection analysis extraction application to the simultaneous determination of nitrophenols. *Anal Chim Acta* 438:103–116. doi:10.1016/S0003-2670(00)01356-8
- Pery DA, Son HJ, Cordova JS, Smith LG, Biris AS (2010) Adsorption analysis of nitrophenol isomers on silver nanostructures by surface-enhanced spectroscopy. *J Colloid Interface Sci* 342:311–319. doi:10.1016/j.jcis.2009.10.053
- Belloli R, Barletta B, Bolzacchini E, Meinardi S, Orlandi M, Rindone B (1999) Determination of toxic nitrophenols in the atmosphere by high-performance liquid chromatography. *J Chromatogr A* 846:277–281. doi:10.1016/S0021-9673(99)00030-8
- Guo X, Wang Z, Zhou S (2004) The separation and determination of nitrophenol isomers by high-performance capillary zone electrophoresis. *Talanta* 64:135–139. doi:10.1016/j.talanta.2004.01.020
- Alizadeh T, Ganjali MR, Norouzi P, Zare M, Zeraatkar A (2009) A novel high selective and sensitive para-nitrophenol voltammetric sensor, based on a molecularly imprinted polymer-carbon paste electrode. *Talanta* 79:1197–1203. doi:10.1016/j.talanta.2009.02.051
- Buchholz KD, Pawliszyn J (1994) Optimization of solid-phase microextraction conditions for determination of phenols. *Anal Chem* 66:160–167. doi:10.1021/ac00073a027
- Rosenstein B, Lewkowicz M, Kao HC, Korniyenko Y (2010) Ballistic transport in graphene beyond linear response. *Phys Rev B*. 81:041416. doi:10.1103/PhysRevB.81.041416
- Erogul S, Bas SZ, Ozmen M, Yildiz S (2015) A new electrochemical sensor based on Fe_3O_4 functionalized graphene oxide-gold nanoparticle composite film for simultaneous determination of catechol and hydroquinone. *Electrochim Acta* 186:302–313. doi:10.1016/j.electacta.2015.10.174
- Arvidsson R, Molander S, Sanden BA (2013) Review of potential environment and health risks of the nanomaterial graphene. *Hum Ecol Risk Assess* 19:873–887. doi:10.1080/10807039.2012.702039
- Brody AL (2006) Nano and food packaging technologies converge. *Food Technol* 60:92–94
- Hu X, Zhou Q (2013) Health and ecosystem risks of graphene. *Chem Rev* 113:3815–3835. doi:10.1021/cr300045n
- Gao W, Majumder M, Alemany LB, Narayanan TN, Ibarra MA, Pradhan BK, Ajayan PM (2011) Engineered graphite oxide materials for application in water purification. *ACS Appl Mater Interfaces* 3:1821–1826. doi:10.1021/am200300u
- Arfin T, Mohammad F (2015) Dendrimer and its role for the advancement of nanotechnology and bioengineering. In: Wythers MC (ed) *Advances in materials science research*, vol 21. Nova Publishers, New York, pp 153–173
- Arfin T, Mohammad F (2014) Thermodynamics and electrochemical characterization of core-shell type gold-coated superparamagnetic iron oxide nanocomposites. *Adv Mat Lett* 5:315–324. doi:10.5185/amlett.2014.amwc.1030
- Jr Hummers WS, Offeman RE (1958) Preparation of graphitic oxide. *J Am Chem Soc* 80:1339–1339. doi:10.1021/ja01539a017
- Cottineau T, Toupin M, Delahaye T, Brousse T, Belanger D (2005) Nanostructured transition metal oxides for aqueous hybrid electrochemical supercapacitors. *Appl Phys A Mater Sci Process* 82:599–606. doi:10.1007/s00339-005-3401-3
- Toupin M, Brousse T, Belanger D (2004) Charge storage mechanism of MnO_2 electrode used in aqueous electrochemical capacitor. *Chem Mater* 16:3184–3190. doi:10.1021/cm049649j
- Li D, Müller MB, Gilje S, Kaner RB, Wallace GG (2008) Processable aqueous dispersions of graphene nanosheets. *Nat Nanotechnol* 3:101–105. doi:10.1038/nnano.2007.451
- Li J, Liu C-Y, Liu L (2012) Au/graphene hydrogel: synthesis, characterization and its use for catalytic reduction of 4-nitrophenol. *J Mater Chem* 22:8426–8430. doi:10.1039/C2JM16386A
- Fernández-Merino MJ, Guardia L, Paredes JI, Villar-Rodil S, Solís-Fernández P, Martínez-Alonso A, Tascón JMD (2010) Vitamin C is an ideal substitute for hydrazine in the reduction of graphene oxide suspensions. *J Phys Chem C* 114:6426–6432. doi:10.1021/jp100603h
- Xu LQ, Yang WJ, Neoh KG, Kang ET, Fu GD (2010) Dopamine-induced reduction and functionalization of graphene oxide nanosheets. *Macromolecules* 43:8336–8339. doi:10.1021/ma101526k
- Arfin T, Kumar C (2014) Synthesis, characterization, conductivity and antibacterial activity of ethyl cellulose manganese (II) hydrogen phosphate. *Anal Bioanal Electrochem* 6:403–421

25. Arfin T, Mohammad F (2016) Electrochemical, antimicrobial and anticancer effect of ethyl cellulose-nickel (II) hydrogen phosphate. *Innov Corros Mater Sci* 6:10–18. doi:[10.2174/2352094906999160307182012](https://doi.org/10.2174/2352094906999160307182012)
26. Xu CY, Zhang PX, Yan L (2001) Blue shift of Raman peak from coated TiO₂ nanoparticles. *J Raman Spectrosc* 32:862–865. doi:[10.1002/jrs.773](https://doi.org/10.1002/jrs.773)
27. Yu PY, Cardona M (1996) *Fundamentals of semiconductors: physics and material properties*. Springer-Verlag, Berlin
28. Gurnathan S, Han JW, Dayem AA, Eppakayala V, Park M-R, Kwon D-N, Kim J-H (2013) Antibacterial activity of dithiothreitol reduced graphene oxide. *J Ind Eng Chem* 19:1280–1288. doi:[10.1016/j.jiec.2012.12.029](https://doi.org/10.1016/j.jiec.2012.12.029)
29. Krishnamoorthy K, Veerapandian M, Mohan R, Kim S-J (2012) Investigation of Raman and photoluminescence studies of reduced graphene oxide sheets. *Appl Phys A Mater Sci Process* 106:501–506. doi:[10.1007/s00339-011-6720-6](https://doi.org/10.1007/s00339-011-6720-6)
30. Shen J, Shi M, Yan B, Ma H, Li N, Hu Y (2010) Ye M (2010) Covalent attaching protein to graphene oxide via diimide-activated amidation. *Colloid Surf B: Biointerfaces* 81(434–438):434. doi:[10.1016/j.colsurfb.2010.07.035](https://doi.org/10.1016/j.colsurfb.2010.07.035)
31. Lu J, Yang J-X, Wang J, Lim A, Wang S, Loh KP (2009) One-pot synthesis of fluorescent carbon nanoribbons, nanoparticles, and graphene by the exfoliation of graphite in ionic liquids. *ACS Nano* 3:2367–2375. doi:[10.1021/nn900546b](https://doi.org/10.1021/nn900546b)
32. Chen WF, Yan LF, Bangal PR (2010) Chemical reduction of graphene oxide to graphene by sulphur-containing compounds. *J Phys Chem C* 114:19885–19890. doi:[10.1021/jp107131v](https://doi.org/10.1021/jp107131v)
33. Song P, Zhang XY, Sun MX, Cui XL, Lin YH (2012) Synthesis of graphene nanosheets via oxalic acid-induced chemical reduction of exfoliated graphite oxide. *RSC Adv* 2:1168–1173. doi:[10.1039/C1RA00934F](https://doi.org/10.1039/C1RA00934F)
34. Stankovich S, Dikin DA, Piner RD, Kohlhaas KA, Kleinhammes A, Jia YY, Wu Y, Nguyen ST, Ruoff RS (2007) Synthesis of graphene-based nanosheets via chemical reduction of exfoliated graphite oxide. *Carbon* 45:1558–1565. doi:[10.1016/j.carbon.2007.02.034](https://doi.org/10.1016/j.carbon.2007.02.034)
35. Park S, Ruoff RS (2009) Chemical methods for the production of graphenes. *Nat Nanotechnol* 4:217–224. doi:[10.1038/nnano.2009.58](https://doi.org/10.1038/nnano.2009.58)
36. Rattana Chaiyakun S, Witit-anun N, Nuntawong N, Chindaudom P, Oaew S, Kedkeaw C, Limsuwan P (2012) Preparation and characterization of graphene oxide nanosheets. *Procedia Eng* 32:759–764. doi:[10.1016/j.proeng.2012.02.009](https://doi.org/10.1016/j.proeng.2012.02.009)
37. Si Y, Samulski ET (2008) Synthesis of water soluble graphene. *Nano Lett.* 8:1679–1682. doi:[10.1021/nl080604h](https://doi.org/10.1021/nl080604h)
38. Ntsewanda B, Mamba BB, Sampath S, Arotiba OA (2012) Electrochemical detection of bisphenol a using graphene-modified glassy carbon electrode. *Int J Electrochem Sci* 7:3501–3512
39. Arfin T, Falch A, Kriek RJ (2012) Evaluation of charge density and the theory for calculating membrane potential for a nano-composite nylon-6,6 nickel phosphate membrane. *Phys Chem Chem Phys* 14:16760–16769. doi:[10.1039/C2CP42683H](https://doi.org/10.1039/C2CP42683H)
40. Arfin T, Mohammad F (2013) Synthesis, characterization and influence of electrolyte solutions towards the electrical properties of nylon-6,6 nickel carbonate membrane: test for the theory of uni-ionic potential based on thermodynamics of irreversible processes. In: Lefebure J (ed) *Halides: chemistry. Physical Properties and Structural Effects*, Nova Publishers, New York, pp 39–66
41. Ma HL, Zhang YW, Hu QH, Yan D, Yu ZZ, Zhai ML (2012) Chemical reduction and removal of Cr(VI) from acidic aqueous solution by ethylenediamine-reduced graphene oxide. *J Mater Chem* 22:5914–5916
42. Li J, Kuang D, Feng Y, Zhang F, Xu Z, Liu M (2012) A graphene oxide-based electrochemical sensor for sensitive determination of 4-nitrophenol. *J Hazard Mater* 201–202:250–259. doi:[10.1016/j.jhazmat.2011.11.076](https://doi.org/10.1016/j.jhazmat.2011.11.076)
43. El Mhammedi MA, Achak M, Bakasse M, Chtaini A (2009) Electrochemical determination of para-nitrophenol at apatite-modified carbon paste electrode: application in river water samples. *J Hazard Mater* 163:323–328. doi:[10.1016/j.jhazmat.2008.06.126](https://doi.org/10.1016/j.jhazmat.2008.06.126)
44. Yang C (2004) Electrochemical determination of 4-nitrophenol using a single-wall carbon nanotube film-coated glassy carbon electrode. *Microchim Acta* 148:87–92. doi:[10.1007/s00604-004-0240-4](https://doi.org/10.1007/s00604-004-0240-4)
45. Huang W, Yang C, Zhang S (2003) Simultaneous determination of 2-nitrophenol and 4-nitrophenol based on the multi-wall carbon nanotubes nafion-modified electrode. *Anal Bioanal Chem* 375:703–707. doi:[10.1007/s00216-002-1745-5](https://doi.org/10.1007/s00216-002-1745-5)
46. Luz RCS, Damos FS, de Oliverira AB, Beck J, Kubota LT (2004) Voltammetric determination of 4-nitrophenol at a lithium tetracyanoethylene (LiTCNE) modified glassy carbon electrode. *Talanta* 64:935–942. doi:[10.1016/j.talanta.2004.04.010](https://doi.org/10.1016/j.talanta.2004.04.010)
47. Zhang D-P, Wu W-L, Long H-Y, Liu Y-C, Yang Z-S (2008) Voltammetric behaviour of o-nitrophenol and damage to DNA. *Int J Mol Sci* 9:316–326. doi:[10.3390/ijms9030316](https://doi.org/10.3390/ijms9030316)
48. Yao C, Sun H, Fu H-F, Tan Z-C (2015) Sensitive simultaneous determination of nitrophenol isomers at poly (p-aminobenzene sulfonic acid) film modified graphite electrode. *Electrochim Acta* 156:163–170. doi:[10.1016/j.electacta.2015.01.043](https://doi.org/10.1016/j.electacta.2015.01.043)
49. Xu X, Liu Z, Zhang X, Duan S, Xu S, Zhou C (2011) β -cyclodextrin functionalized mesoporous silica for electrochemical selective sensor: simultaneous determination of nitrophenol isomers. *Electrochim Acta* 58:142–149. doi:[10.1016/j.electacta.2011.09.015](https://doi.org/10.1016/j.electacta.2011.09.015)
50. Chu L, Han L, Zhang X (2011) Electrochemical simultaneous determination of nitrophenol isomers at nano-gold modified glassy carbon electrode. *J Appl Electrochem* 41:687–694. doi:[10.1007/s10800-011-0281-4](https://doi.org/10.1007/s10800-011-0281-4)
51. Liu Z, Ma X, Zhang H, Lu W, Ma H, Hou S (2012) Simultaneous determination of nitrophenol isomers based on β -cyclodextrin functionalized reduced graphene oxide. *Electroanal* 24:1178–1185. doi:[10.1002/elan.201100735](https://doi.org/10.1002/elan.201100735)
52. Luo L-Q, Zou X-L, Ding Y-P, Wu Q-S (2008) Derivative voltammetric direct simultaneous determination of nitrophenol isomers at a carbon nanotube modified electrode. *Sensor Actuat B Chem* 135:61–65. doi:[10.1016/j.snb.2008.07.019](https://doi.org/10.1016/j.snb.2008.07.019)
53. Tang J, Zhang L, Han G, Liu Y, Tang W (2015) Graphene-chitosan composite modified electrode for simultaneous detection of nitrophenol isomers. *J Electrochem Soc* 162:B267–B274. doi:[10.1149/2.0811510jes](https://doi.org/10.1149/2.0811510jes)